Developmental Biology 496 (2023) 63–72

Contents lists available at ScienceDirect

Developmental Biology

journal homepage: www.elsevier.com/locate/developmentalbiology

Analysis of Cre lines for targeting embryonic airway smooth muscle

Katharine Goodwin [a], Celeste M. Nelson [b,c,*]

[a] Lewis-Sigler Institute for Integrative Genomics, Princeton University, Princeton, NJ, 08544, USA
[b] Department of Chemical and Biological Engineering, Princeton University, Princeton, NJ, 08544, USA
[c] Department of Molecular Biology, Princeton University, Princeton, NJ, 08544, USA

ARTICLE INFO

Keywords:
Mechanical stress
Morphodynamics
Morphogenesis

ABSTRACT

During development of the embryonic mouse lung, the pulmonary mesenchyme differentiates into smooth muscle that wraps around the airway epithelium. Inhibiting smooth muscle differentiation leads to cystic airways, while enhancing it stunts epithelial branching. These findings support a conceptual model wherein the differentiation of smooth muscle sculpts the growing epithelium into branches at precise positions and with stereotyped morphologies. Unfortunately, most approaches to manipulate the differentiation of airway smooth muscle rely on pharmacological or physical perturbations that are conducted *ex vivo*. Here, we explored the use of diphtheria toxin-based genetic ablation strategies to eliminate airway smooth muscle in the embryonic mouse lung. Surprisingly, neither airway smooth muscle wrapping nor epithelial branching were affected in embryos in which the expression of diphtheria toxin or its receptor were driven by several different smooth muscle-specific Cre lines. Close examination of spatial patterns of Cre activity in the embryonic lung revealed that none of these commonly used Cre lines target embryonic airway smooth muscle robustly or specifically. Our findings demonstrate the need for airway smooth muscle-specific Cre lines that are active in the embryonic lung, and serve as a resource for researchers contemplating the use of these commonly used Cre lines for studying embryonic airway smooth muscle.

1. Introduction

During embryonic development, smooth muscle and similar contractile cell types help to shape their adjacent epithelia into complex three-dimensional shapes (Donadon and Santoro, 2021; Jaslove and Nelson, 2018). For example, smooth muscle influences morphogenesis of the epithelia of the mammalian lung (Danopoulos et al., 2018; Goodwin et al., 2019; Kim et al., 2015), digestive tract (Shyer et al., 2013; Yang et al., 2021), and epididymis (Hirashima, 2014). Smooth muscle can be experimentally manipulated to test its roles in epithelial morphogenesis. Pharmacological agents that target signaling pathways known to affect smooth muscle differentiation or contraction can be used to prevent smooth muscle differentiation, induce ectopic smooth muscle wrapping, or tune smooth muscle contractility *ex vivo* (Goodwin et al., 2019; Huycke et al., 2019; Kim et al., 2015). However, these approaches are not cell type-specific and can have off-target effects. Alternatively, smooth muscle can be dissected away from its adjacent epithelium to reveal how it influences morphogenesis mechanically (Goodwin et al., 2022b; Goodwin et al., 2019; Huycke et al., 2019; Kim et al., 2015; Shyer et al., 2013). Once the mesenchyme has been removed, smooth muscle wrapping can be mimicked using physical manipulations to define whether mechanical constraints are sufficient to produce a given epithelial morphology (Shyer et al., 2013). However, these approaches are destructive and cannot be carried out *in vivo*. Furthermore, physical dissections are typically limited to acute perturbations and provide little opportunity for observing effects on the epithelium over longer timescales.

Genetic manipulations (e.g., deletions or mutations) are generally considered to be the gold standard for interrogating biological systems and, in principle, could be used to assess the role of smooth muscle *in vivo*. However, these approaches have not always produced clean or expected results when used to study smooth muscle. Mice that lack markers of contractile smooth muscle, such as *Acta2* (smooth muscle actin; αSMA), *Cnn1* (calponin-1), or *Tagln* (transgelin or SM22α), are all viable (Feng et al., 2019; Schildmeyer et al., 2000; Zhang et al., 2001). Targeting upstream regulators of smooth muscle, rather than marker genes,

Abbreviations: αSMA, α-smooth muscle actin; DT, diphtheria toxin; DTR, diphtheria toxin receptor; SRF, serum response factor; UMAP, uniform manifold approximation and projection.

* Corresponding author. 303 Hoyt Laboratory, William Street, Princeton University, Princeton, NJ, 08544, USA.
E-mail address: celesten@princeton.edu (C.M. Nelson).

https://doi.org/10.1016/j.ydbio.2023.01.008
Received 4 August 2022; Received in revised form 9 January 2023; Accepted 22 January 2023
Available online 25 January 2023

is an alternative approach. However, genetic manipulations have revealed that embryonic airway smooth muscle is surprisingly plastic in mice. Deleting serum response factor, which regulates the smooth muscle differentiation program along with its cofactor myocardin (Chen et al., 2002; Du et al., 2003; Wang et al., 2003), fails to ablate airway smooth muscle and instead leads to a loss of contractile smooth muscle markers and formation of an immature smooth muscle layer around the airway epithelium (Goodwin et al., 2022a). Similarly, deleting myocardin from the embryonic pulmonary mesenchyme also leads to a loss of contractile smooth muscle markers without affect branching morphogenesis of the adjacent epithelium (Young et al., 2020). These findings suggest that genetically disrupting a single transcription factor is unlikely to result in loss of smooth muscle tissue.

A final alternative approach to manipulate smooth muscle genetically is to take advantage of diphtheria toxin-based ablation systems (Buch et al., 2005; Ivanova et al., 2005). These mice are genetically engineered to express either diphtheria toxin (DT; $DTA^{fl/fl}$) or the human diphtheria toxin receptor (DTR; $iDTR^{fl/fl}$) in a Cre-recombinase-inducible manner. Once inside the cell, DT terminates protein synthesis and thus promotes apoptotic cell death (Honjo et al., 1971). Cre-induced expression of DTA results in intracellular DT *in vivo* without further intervention, whereas Cre-induced expression of DTR requires treatment with DT and receptor-mediated endocytosis. To target airway smooth muscle (or smooth muscle generally), there are a variety of mouse lines in which Cre is driven by markers of contractile smooth muscle, including *Acta2-Cre* (LeBleu et al., 2013), *Myh11-Cre* (Xin et al., 2002), and *Tagln-Cre*

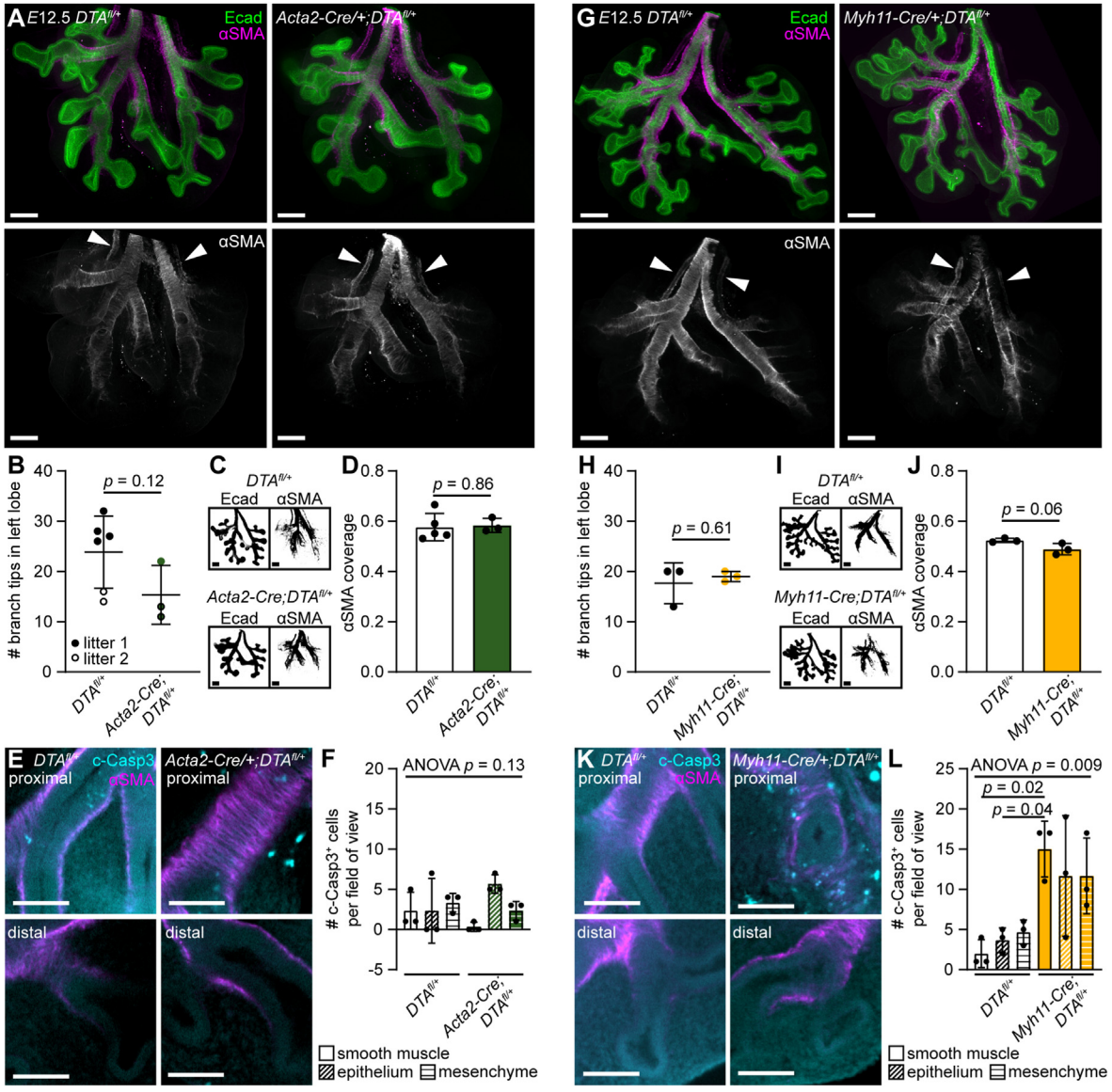

Fig. 1. Using *Acta2-Cre* and *Myh11-Cre* to drive expression of DT does not affect airway smooth muscle wrapping or epithelial branching morphogenesis at the early pseudoglandular stage (*E*12.5). (**A**) *E*12.5 $DTA^{fl/+}$ and *Acta2-Cre;*$DTA^{fl/+}$ lungs immunostained for Ecad and αSMA. Scale bars indicate 100 μm. (**B**) Number of branches in the left lobe. (**C**) Thresholded z-projections of images of lungs immunostained for Ecad and αSMA. Scale bars indicate 100 μm. (**D**) Smooth muscle coverage, defined as the projected area of αSMA staining divided by that of Ecad staining. (**E**) *E*12.5 $DTA^{fl/+}$ and *Acta2-Cre;*$DTA^{fl/+}$ lungs immunostained for αSMA and cleaved Casp3 (c-Casp3). Proximal and distal regions are shown. Scale bars indicate 50 μm. (**F**) Number of c-$Casp3^{+}$ cells per field of view in the smooth muscle, epithelium, and mesenchyme. (**G**) *E*12.5 $DTA^{fl/+}$ and *Myh11-Cre;*$DTA^{fl/+}$ lungs immunostained for Ecad and αSMA. Scale bars indicate 100 μm. (**H**) Number of branches in the left lobe. (**I**) Thresholded z-projections of images of lungs immunostained for Ecad and αSMA. Scale bars indicate 100 μm. (**J**) Smooth muscle coverage, defined as the projected area of αSMA staining divided by that of Ecad staining. (**K**) *E*12.5 $DTA^{fl/+}$ and *Myh11-Cre;*$DTA^{fl/+}$ lungs immunostained for αSMA and c-Casp3. Proximal and distal regions are shown. Scale bars indicate 50 μm. (**L**) Number of c-$Casp3^{+}$ cells per field of view in the smooth muscle, epithelium, and mesenchyme. *p* values were obtained using unpaired t-tests unless otherwise indicated. Error bars show s.d.

(Holtwick et al., 2002). Diptheria toxin-based ablation systems have been used to eliminate airway epithelial stem cells (Zuo et al., 2015) and pericytes (Hung et al., 2017) of the mouse lung. Surprisingly, in explanted lungs that express DTR under the control of *Myh11-Cre*, treatment with DT does not significantly affect the wrapping of airway smooth muscle. One possible explanation for the inability of DT to ablate airway smooth muscle in the embryo is the fact that *Myh11-Cre* activity is restricted to mature contractile smooth muscle, whereas the embryonic airways are initially wrapped by immature smooth muscle (Goodwin et al., 2022a, 2022b; Goodwin et al., 2019). In contrast, using *Acta2-Cre* to drive the expression of DTR leads to a moderate loss of smooth muscle wrapping and alteration of epithelial morphology (Goodwin et al., 2019), perhaps because *Acta2* is expressed at earlier stages of smooth muscle differentiation (Goodwin et al., 2022a). Whether these Cre lines would generate a stronger phenotype using $DTA^{fl/fl}$ mice is unknown. *Tagln* is considered to be an early marker for smooth muscle (Solway et al., 1995), but experiments using *Tagln-Cre* to ablate airway smooth muscle via DT expression have not been reported.

Here, we investigated the extent to which three smooth muscle-specific Cre lines, *Acta2-Cre*, *Myh11-Cre*, and *Tagln-Cre*, could be used to ablate airway smooth muscle *in vivo* during embryonic lung development. We used *Acta2-Cre* and *Myh11-Cre* to drive the expression of DT and found that smooth muscle wrapping is unaffected at both early and late stages of epithelial morphogenesis. In contrast, using *Tagln-Cre* to drive the expression of DT caused embryonic lethality prior to lung formation. To circumvent this complication, we instead used *Tagln-Cre* to drive the expression of DTR. We found that treating *E*11.5 *Tagln-Cre;iDTR*$^{fl/+}$ lung explants with DT is not sufficient to ablate smooth

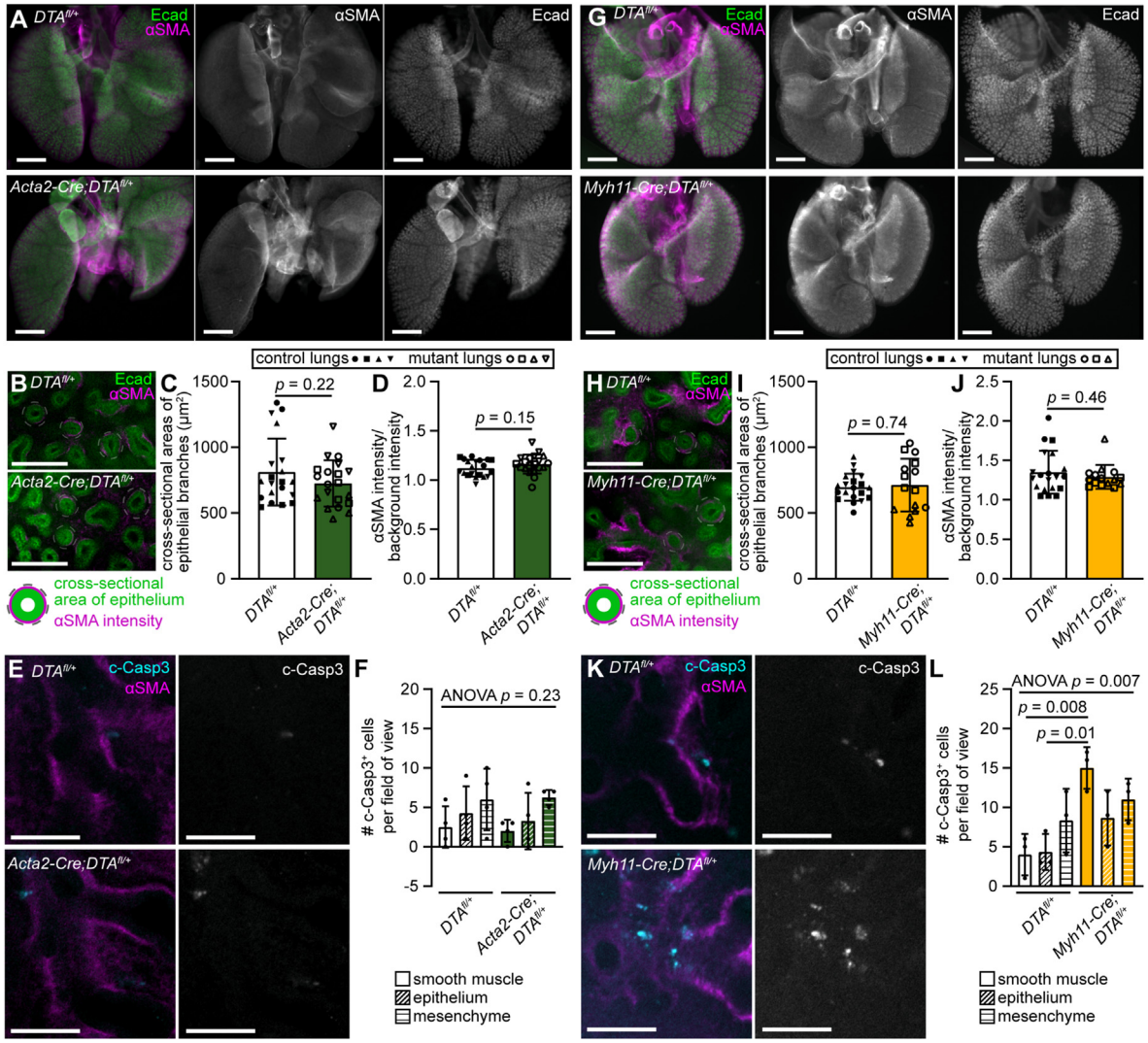

Fig. 2. Using *Acta2-Cre* and *Myh11-Cre* to drive expression of DT does not affect airway smooth muscle wrapping or epithelial branching morphogenesis at the late pseudoglandular stage (*E*15.5). (**A**) *E*15.5 $DTA^{fl/+}$ and *Acta2-Cre;*$DTA^{fl/+}$ lungs immunostained for Ecad and αSMA. Scale bars indicate 500 μm. (**B**) Zoomed-in views of the distal airways of *E*15.5 $DTA^{fl/+}$ and *Acta2-Cre;*$DTA^{fl/+}$ lungs immunostained for αSMA and Ecad. Dashed lines indicate cross-sections of branches where area and αSMA intensity were measured, as detailed in the schematic. Scale bars indicate 100 μm. (**C**) Cross-sectional areas of epithelial branches. Measurements from the same lung have matching symbol shapes. (**D**) αSMA immunofluorescence intensity around epithelial branches. (**E**) *E*15.5 $DTA^{fl/+}$ and *Acta2-Cre;*$DTA^{fl/+}$ lungs immunostained for αSMA and cleaved Casp3 (c-Casp3). Scale bars indicate 50 μm. (**F**) Number of c-Casp3^{+} cells per field of view in the smooth muscle, epithelium, and mesenchyme. (**G**) *E*15.5 $DTA^{fl/+}$ and *Myh11-Cre;*$DTA^{fl/+}$ lungs immunostained for Ecad and αSMA. Scale bars indicate 500 μm. (**H**) Zoomed-in views of the distal airways of *E*15.5 $DTA^{fl/+}$ and *Myh11-Cre;*$DTA^{fl/+}$ lungs immunostained for αSMA and Ecad. Dashed lines indicate cross-sections of branches where area and αSMA intensity were measured, as detailed in the schematic. Scale bars indicate 100 μm. (**I**) Cross-sectional areas of epithelial branches. Measurements from the same lung have matching symbol shapes. (**J**) αSMA immunofluorescence intensity around epithelial branches. (**K**) *E*15.5 $DTA^{fl/+}$ and *Myh11-Cre;*$DTA^{fl/+}$ lungs immunostained for αSMA and c-Casp3. Scale bars indicate 50 μm. (**L**) Number of c-Casp3^{+} cells per field of view in the smooth muscle, epithelium, and mesenchyme. *p* values were obtained using unpaired t-tests unless otherwise indicated. Error bars show s.d.

muscle. To determine why we were unable to ablate smooth muscle using these Cre drivers, we examined patterns of Cre expression using a fluorescent reporter line. Surprisingly, we found that none of these drivers results in either sufficient or specific expression of Cre in embryonic airway smooth muscle. Our findings highlight the importance of using reporters to confirm patterns of Cre activity, and emphasize the need for a smooth muscle-specific Cre that is robustly expressed in embryonic smooth muscle.

2. Materials and methods

2.1. Mice

Breeding of *Rosa26*-mTmG (hereafter referred to as mTmG; JAX 007676), *Rosa26-iDTR* (*iDTR*$^{fl/fl}$; JAX 007900), *Rosa26-DTA* (*DTA*$^{fl/fl}$; JAX 009669), *Acta2-Cre* (JAX 029925), *Myh11-Cre-EGFP* (*Myh11-Cre*; JAX 007742), and *Tagln-Cre* (JAX 017491) mice and isolation of embryos were carried out in accordance with institutional guidelines following the NIH Guide for the Care and Use of Laboratory Animals and approved by Princeton's Institutional Animal Care and Use Committee. To label Cre-expressing cells, *Acta2-Cre*, *Myh11-Cre*, or *Tagln-Cre* males were mated to *mTmG* females and embryos were isolated at *E*12.5 or *E*15.5. To ablate Cre-expressing cells, *Acta2-Cre*, *Myh11-Cre*, or *Tagln-Cre* males were mated to *DTA*$^{fl/fl}$ females. For crosses with *Acta2-Cre* and *Myh11-Cre* males, embryos were isolated at *E*12.5 or *E*15.5. For crosses with *Tagln-Cre* males, embryos were isolated at *E*10.5, *E*11.5, or *E*12.5, but no Cre-positive embryos were found. To ablate Cre-expressing cells in explants cultured *ex vivo* in the presence of DT, *Tagln-Cre* males were crossed to *iDTR*$^{fl/fl}$ females and embryos were isolated at *E*11.5. Genotyping was carried out by isolating DNA from the head of each embryo, followed by PCR amplification of the Cre product and gel electrophoresis. The forward primer sequence for Cre was GCATTACCGGTCGATGCAACGAGTGATGAG and the reverse primer sequence was GAGTGAACGAACCTGGTCGAAATCAGTGCG.

2.2. Tissue sectioning, immunofluorescence staining, and imaging

Isolated lungs were fixed in 4% paraformaldehyde in PBS at room temperature for either 15 min for *E*12.5 lungs or 30 min for *E*15.5 lungs. Samples were washed four times for 15 min each with PBST (0.1% Triton X-100 in PBS) and then blocked with 5% goat serum and 0.1% BSA. *E*15.5 lungs were additionally washed overnight with PBST prior to blocking. Samples were then incubated with primary antibodies against αSMA (Sigma a5228, 1:400), GFP (Invitrogen A-11122, 1:500), cleaved caspase-3 (Cell Signaling 9661, 1:200), or E-cadherin (Cell Signaling 3195, 1:200 or Invitrogen 13–1900, 1:200), followed by incubation with Alexa Fluor-conjugated secondary antibodies (1:200; Thermo Fisher Scientific) and Hoechst (1:1000). Sections on slides were then mounted in Fluorosave. Whole lungs were dehydrated in a methanol series and cleared with Murray's clear (1:2 ratio of benzyl alcohol to benzyl benzoate). Samples were imaged using a spinning disk confocal (BioVision X-Light V2) fitted to an inverted microscope.

2.3. Organ culture and live imaging

Lungs were dissected in PBS and cultured on porous membranes (nucleopore polycarbonate track-etch membrane, 8 μm pore size, 25 mm diameter; Whatman) in DMEM/F12 medium (without HEPES) supplemented with 5% fetal bovine serum (FBS, heat inactivated; Atlanta Biologicals) and antibiotics (50 units/ml of penicillin and streptomycin). *E*11.5 lungs were isolated from *iDTR*$^{fl/fl}$ females bred to *Tagln-Cre* males, and then treated with 0.2 ng/μl DT (Sigma-Aldrich). Before adding it to the culture medium, DT was unnicked by incubating with trypsin at a ratio of 1:10,000 in PBS for 15 min at 37 °C. *iDTR*$^{fl/+}$ littermates were used as controls.

2.4. Image and statistical analysis

All measurements were made in Fiji. Numbers of branches per lung were counted, focusing on only the left lobe for *E*12.5 lungs and the entire lung for explants. Smooth muscle coverage was estimated by generating thresholded images of Ecad and αSMA immunofluorescence, obtaining the area of each, and dividing the αSMA$^+$ area by the Ecad$^+$ area. The numbers of cleaved Casp3$^+$ cells and GFP$^+$ cells in αSMA$^+$ smooth muscle, Ecad$^+$ epithelium, and αSMA$^-$, Ecad$^-$, Hoechst$^+$ mesenchyme were counted in multi-channel confocal z-stacks with a field of view of ~185 × 185 μm. Epithelial cross-sectional areas and αSMA intensity around branches at *E*15.5 were measured manually by tracing the circumference of the epithelium and recording intensity values in a 10-pixel-thick line. Intensity values were normalized to background intensity. Statistical analyses were carried out in GraphPad Prism. Comparisons between two samples were performed using unpaired *t*-test. Comparisons of more than two samples were performed using one-way ANOVA with pairwise *p* values obtained using Tukey's multiple comparisons test.

2.5. scRNA-seq analysis

ScRNA-seq datasets were downloaded from GEO [*E*11.5 mouse lung: GSE153069 (Goodwin et al., 2022a), *E*14.5 mouse intestine: GSE154007 (Fazilaty et al., 2021)] and processed using the standard Seurat pipeline (Stuart et al., 2019). Cell types were identified based on known markers, and uniform manifold approximation and projection (UMAP) plots were generated and color-coded based on the expression of *Acta2*, *Myh11*, and *Tagln*.

2.6. KEY RESOURCES TABLE

KEY RESOURCES TABLE.

REAGENT or RESOURCE	SOURCE	IDENTIFIER
Antibodies		
Mouse monoclonal αSMA antibody	Sigma	a5228
Rabbit monoclonal E-cadherin antibody	Cell Signaling	3195
Rat monoclonal E-cadherin antibody	Invitrogen	13–1900
Rabbit polyclonal cleaved Caspase3 antibody	Cell Signaling	9661
Rabbit polyclonal GFP antibody	Invitrogen	A-11122
Goat anti-Mouse IgG1 Cross-Adsorbed Secondary Antibody, Alexa Fluor 647	Invitrogen	A-21240
Goat anti-Rat IgG (H + L) Cross-Adsorbed Secondary Antibody, Alexa Fluor 488	Invitrogen	A-11006
Goat anti-Rat IgG (H + L) Cross-Adsorbed Secondary Antibody, Alexa Fluor 594	Invitrogen	A-11007
Goat anti-Rabbit IgG (H + L) Cross-Adsorbed Secondary Antibody, Alexa Fluor 594	Invitrogen	A-11012
Goat anti-Rabbit IgG (H + L) Cross-Adsorbed Secondary Antibody, Alexa Fluor 647	Invitrogen	A-21244
Chemicals, Peptides, and Recombinant Proteins		
Diphtheria toxin	Sigma-Aldrich	D0564
Deposited Data		
scRNA-seq data of *E*11.5 mouse lungs	Goodwin et al. (2022a)	GEO: GSE153069
scRNA-seq data of *E*14.5 mouse intestine	Fazilaty et al. (2021)	GEO: GSE154007
Experimental Models: Organisms/Strains		
Mouse: B6.129(Cg)-*Gt(ROSA)26Sor*$^{tm4(ACTB-tdTomato,-EGFP)Luo}$/J	The Jackson Laboratory	JAX: 007676
Mouse: C57BL/6-Gt*(ROSA)26Sor*$^{tm1(HBEGF)Awai}$/J	The Jackson Laboratory	JAX: 007900
Mouse: B6.129P2-*Gt(ROSA)26Sor*$^{tm1(DTA)Lky}$/J	The Jackson Laboratory	JAX: 009669
Mouse: B6.FVB-Tg(Acta2-cre)1Rkl/J	The Jackson Laboratory	JAX: 029925
Mouse: B6.Cg-Tg(Myh11-cre,-EGFP)2Mik/J		JAX: 007742

(*continued on next page*)

(*continued*)

REAGENT or RESOURCE	SOURCE	IDENTIFIER
Mouse: B6.Cg-Tg(Tagln-cre)1Her/J	The Jackson Laboratory	JAX: 017491
Oligonucleotides		
Primer: Cre, Forward: GCATTACCGGTCGATGCAACGAGTGATGAG	Devenport Lab	N/A
Primer: Cre, Reverse: GAGTGAACGAACCTGGTCGAAATCAGTGCG	Devenport Lab	N/A
Software and Algorithms		
ImageJ	Schneider et al. (2012)	https://imagej.nih.gov/ij/
R	R Foundation for Statistical Computing	N/A
Seurat	Butler et al. (2018)	https://satijalab.org/seurat/

3. Results and discussion

3.1. DT-based strategies using smooth muscle-specific Cre lines to genetically ablate embryonic airway smooth muscle in vivo are ineffective

To ablate smooth muscle cells *in vivo*, we crossed *Acta2-Cre* or *Myh11-Cre* males to $DTA^{fl/fl}$ females. In the embryonic lung, this approach should result in the expression of DT specifically in smooth muscle cells, leading to cell death and eliminating smooth muscle wrapping around the embryonic airway epithelium. We isolated embryos at *E*12.5, during the early (pseudoglandular) stage of branching morphogenesis, and carried out immunofluorescence analysis for E-cadherin (Ecad) and α-smooth muscle actin (αSMA). We found that smooth muscle wrapping and branching morphogenesis were identical in *Acta2-Cre;*$DTA^{fl/+}$ mutants as compared to $DTA^{fl/+}$ controls (Fig. 1A). The numbers of branch tips (Fig. 1B) and the proportion of the epithelium covered by smooth muscle were statistically indistinguishable between mutants and controls (Fig. 1C-D). To determine whether smooth muscle cells were undergoing apoptosis in response to DT expression, we examined the localization of cleaved caspase 3 (c-Casp3). We found that apoptotic cells were randomly distributed throughout the lung, with no clear enrichment in the smooth muscle layer (Fig. 1E–F).

We found similar results with *Myh11-Cre*: smooth muscle wrapping and airway epithelial branching were indistinguishable from controls at *E*12.5 (Fig. 1G–J). In this case, however, we observed increased levels of c-Casp3 in the smooth muscle layer of *Myh11-Cre;*$DTA^{fl/+}$ mutants as compared to $DTA^{fl/+}$ controls (Fig. 1K-L). Nonetheless, this level of apoptosis was insufficient to cause appreciable changes in smooth muscle wrapping. We also observed slightly increased levels of apoptosis in the epithelium and αSMA^{-} mesenchyme in *Myh11-Cre;*$DTA^{fl/+}$ mutants as compared to $DTA^{fl/+}$ controls, but these differences were not significant (Fig. 1K-L). These data show that DT expression driven by *Acta2-Cre* or *Myh11-Cre* is insufficient to ablate embryonic airway smooth muscle or influence branching morphogenesis of the airway epithelium.

To confirm these conclusions, we isolated lungs from embryos at *E*15.5, at the end of the pseudoglandular stage when the epithelium is in the final stages of branching morphogenesis. In *Acta2-Cre;*$DTA^{fl/+}$ lungs, there are no appreciable changes in smooth muscle wrapping or airway epithelial branching at *E*15.5 (Fig. 2A). Quantification of the cross-sectional area of epithelial branches and the intensity of αSMA staining around them revealed no differences between mutants and controls (Fig. 2B–D). Furthermore, the levels of c-Casp3 immunostaining in the smooth muscle layer and throughout the lung were similar in *Acta2-Cre;*$DTA^{fl/+}$ lungs as in $DTA^{fl/+}$ controls (Fig. 2E–F). We found a similar lack of phenotype at *E*15.5 in *Myh11-Cre;*$DTA^{fl/+}$ mutants: epithelial branching was normal and the smooth muscle layer appeared intact (Fig. 2G–J). Similar to *E*12.5 lungs, *E*15.5 *Myh11-Cre;*$DTA^{fl/+}$ lungs showed an increase in c-Casp3 immunostaining in the smooth muscle layer compared to $DTA^{fl/+}$ controls, but also exhibited slightly higher levels of apoptosis in the epithelium and mesenchyme (Fig. 2K-L). Overall, we found that expressing DT using *Acta2-Cre* or *Myh11-Cre* is insufficient to ablate embryonic airway smooth muscle and, consequently, has no effect on branching morphogenesis of the airway epithelium.

3.2. A DT-based strategy using Tagln-Cre to genetically ablate airway smooth muscle ex vivo is ineffective

Since we were unable to ablate airway smooth muscle using either *Acta2-Cre* or *Myh11-Cre*, we turned to *Tagln-Cre* (Solway et al., 1995), which was previously reported to be expressed in nascent airway smooth muscle cells at *E*11.5 (Goss et al., 2011). When we crossed *Tagln-Cre* males to $DTA^{fl/fl}$ females, we found no Cre^{+} embryos at *E*10.5, *E*11.5, or *E*12.5, suggesting that this genotype is embryonic lethal prior to the onset of organogenesis. We therefore used an alternative approach to ablate Cre-expressing cells. We crossed *Tagln-Cre* males to $iDTR^{fl/fl}$ females to generate embryos that produce DTR in cells that express *Tagln*. We isolated embryos at *E*11.5 and cultured lung explants for 24 h *ex vivo* in the presence of DT to selectively kill cells expressing DTR. This approach did not appreciably affect either smooth muscle wrapping or epithelial morphogenesis (Fig. 3A–B). The number, lengths, and widths of branches were similar in mutants and controls (Fig. 3C–E), as was smooth muscle coverage of the epithelium (Fig. 3F–G). The levels of apoptosis in the smooth muscle, epithelium, and mesenchyme were also indistinguishable between mutants and controls (Fig. 3H–I). Relatively high numbers of $c\text{-}Casp3^{+}$ cells were detected in all tissues in both sets of samples, presumably because they were cultured *ex vivo*. Overall, driving DTR using *Tagln-Cre* and treating explanted lungs with DT does not selectively ablate airway smooth muscle.

3.3. Smooth muscle-specific Cre lines show either sparse or non-specific recombination of the mTmG reporter

To determine why we were unable to ablate embryonic airway smooth muscle using any of these smooth muscle-specific Cre lines to drive the expression of DT or DTR, we crossed each Cre line to mice harboring the mTmG reporter. We used the resulting embryos to examine the patterns of Cre expression in the lung and intestine, which is also wrapped by a layer of smooth muscle during embryonic development (Huycke et al., 2019; Shyer et al., 2013). We isolated lungs and intestines from embryos at *E*12.5 and used immunofluorescence analysis to localize GFP^{+} and αSMA^{+} cells. We found that *E*12.5 *Acta2-Cre;mTmG* lungs had very few GFP^{+} cells within the airway smooth muscle layer (Fig. 4A–B). This low level of Cre activity was not unique to the embryonic lung, as we found a similar low incidence of GFP^{+} cells in the embryonic intestine (Fig. 4C). Quantification of the number of GFP^{+} cells in the smooth muscle, epithelium, and mesenchyme revealed no statistically significant differences in either the lung or the intestine (Fig. 4D).

Lungs and intestines isolated from *E*12.5 *Myh11-Cre;mTmG* embryos both had a greater number of GFP^{+} cells than those isolated from *Acta2-Cre;mTmG* embryos, but the number of GFP^{+} cells remained far lower than the number of αSMA^{+} cells (Fig. 4E–H). Additionally, GFP^{+} cells were present in the airway epithelium and throughout the lung mesenchyme in locations that lacked αSMA immunofluorescence (Fig. 4H). GFP^{+} cells were not detected in the epithelium or the mesenchyme of the intestine, suggesting that *Myh11-Cre* may be suitable for studies of intestinal development. Finally, we examined lungs and intestines isolated from *E*12.5 *Tagln-Cre;mTmG* embryos and found surprising patterns of GFP^{+} cells. In both the lung and the intestine, GFP^{+} cells were located throughout the mesenchyme, sparsely within the smooth muscle, and

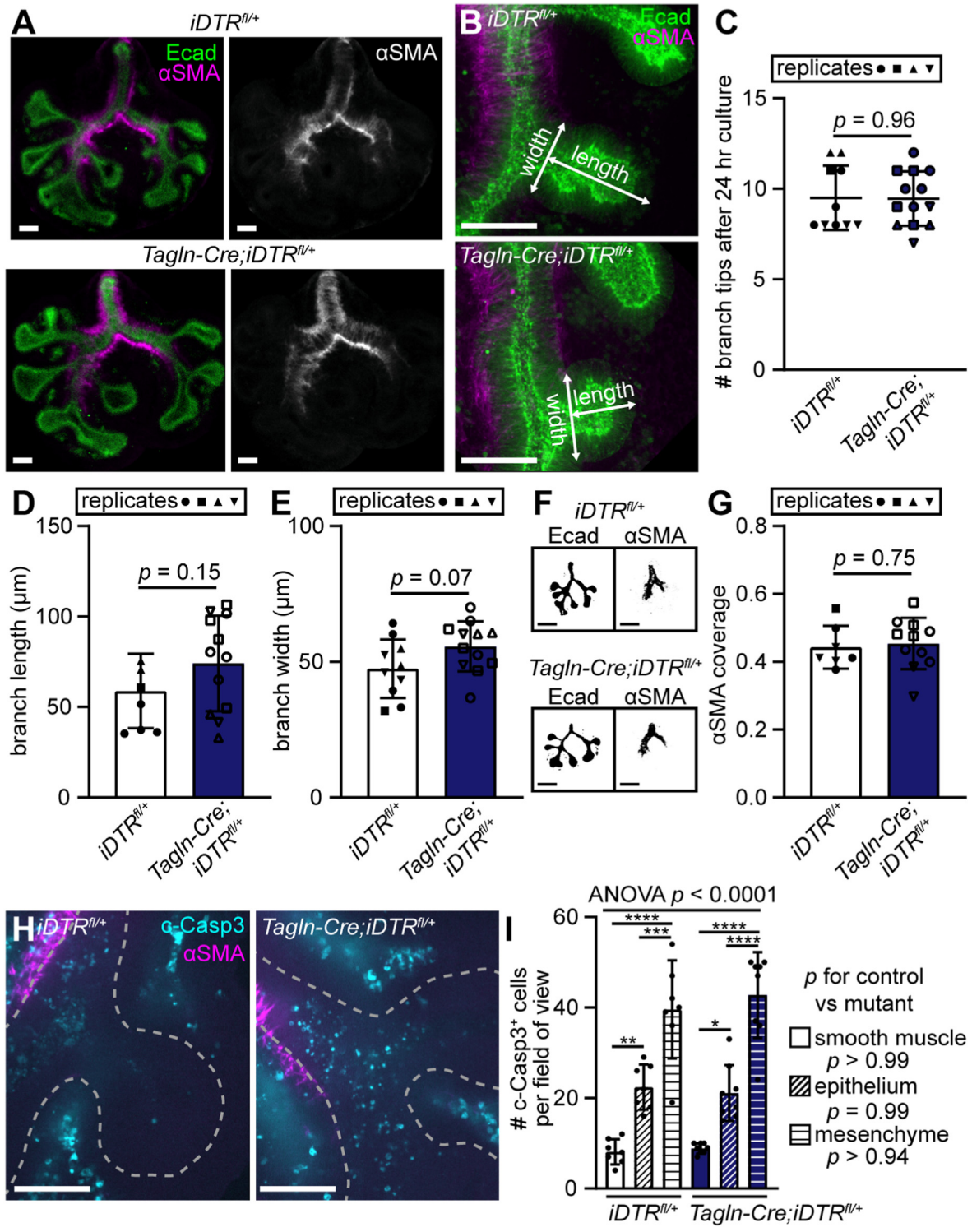

Fig. 3. DT-mediated ablation of airway smooth muscle cells *ex vivo* with *Tagln-Cre* is ineffective. (**A-B**) Confocal z-projections of control and *Tagln-Cre;iDTR*$^{fl/+}$ lungs isolated at *E*11.5 and cultured *ex vivo* for 24 h in the presence of 0.2 ng/ml DT and then immunostained for Ecad and αSMA. Scale bars indicate 50 μm. (**C**) Number of branch tips in explants after 24 h. Lungs from the same replicate have matching symbol shapes. (**D-E**) Length and width of branches as indicated in (B). (**F**) Thresholded z-projections of images of lungs immunostained for Ecad and αSMA. Scale bars indicate 50 μm. (**G**) Smooth muscle coverage, defined as the projected area of αSMA staining divided by that of Ecad staining. (**H**) Single confocal slices of control and *Tagln-Cre;iDTR*$^{fl/+}$ lungs cultured in the presence of DT and then immunostained for αSMA and cleaved Casp3 (c-Casp3). Dashed line indicates the outline of the epithelium. Scale bars indicate 50 μm. (**I**) Number of c-Casp3^{+} cells per field of view in the smooth muscle, epithelium, and mesenchyme. *p* values were obtained using unpaired t-tests unless otherwise indicated. Error bars show s.d.

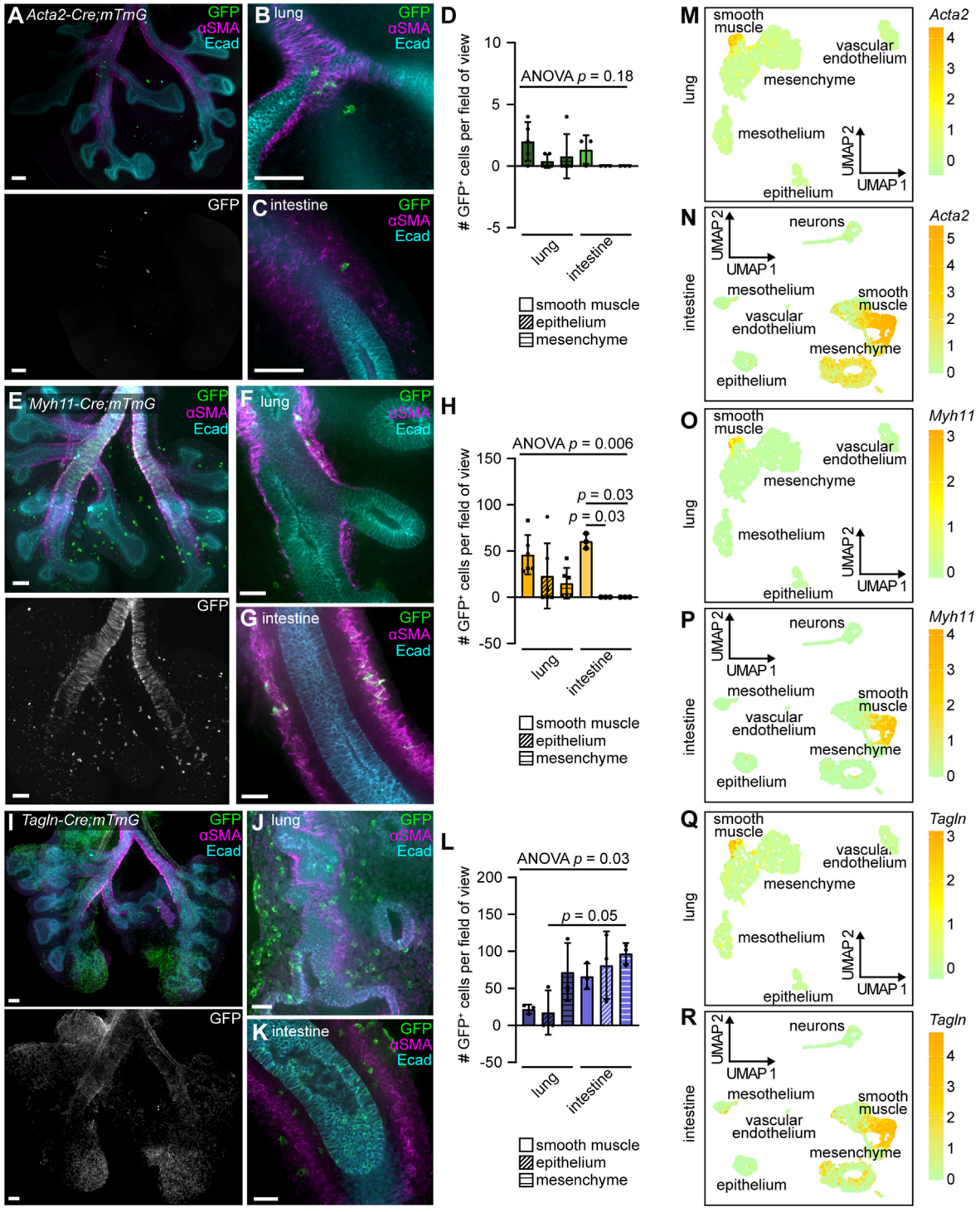

Fig. 4. Expression patterns of three smooth muscle-specific Cre lines in the embryonic lung and intestine at *E*12.5. (**A-B**) *E*12.5 *Acta2-Cre;mTmG* lungs immunostained for GFP, Ecad, and αSMA. (**C**) *E*12.5 *Acta2-Cre;mTmG* intestine immunostained for GFP, Ecad, and αSMA. (**D**) Number of GFP^+ cells per field of view in the smooth muscle, epithelium, and mesenchyme of the lungs and intestine. (**E-F**) *E*12.5 *Myh11-Cre;mTmG* lungs immunostained for GFP, Ecad, and αSMA. (**G**) *E*12.5 *Myh11-Cre;mTmG* intestine immunostained for GFP, Ecad, and αSMA. (**H**) Number of GFP^+ cells per field of view in the smooth muscle, epithelium, and mesenchyme of the lungs and intestine. (**I-J**) *E*12.5 *Tagln-Cre;mTmG* lungs immunostained for GFP, Ecad, and αSMA. (**K**) *E*12.5 *Tagln-Cre;mTmG* intestine immunostained for GFP, Ecad, and αSMA. (**L**) Number of GFP^+ cells per field of view in the smooth muscle, epithelium, and mesenchyme of the lungs and intestine. (**M-R**) UMAPs of scRNA-seq data collected from *E*11.5 lungs and *E*14.5 intestines color-coded to show the expression of *Acta2*, *Myh11*, and *Tagln*. Clusters are labelled by cell type. *p* values obtained using ANOVA. Error bars show s.d. Scale bars indicate 50 μm.

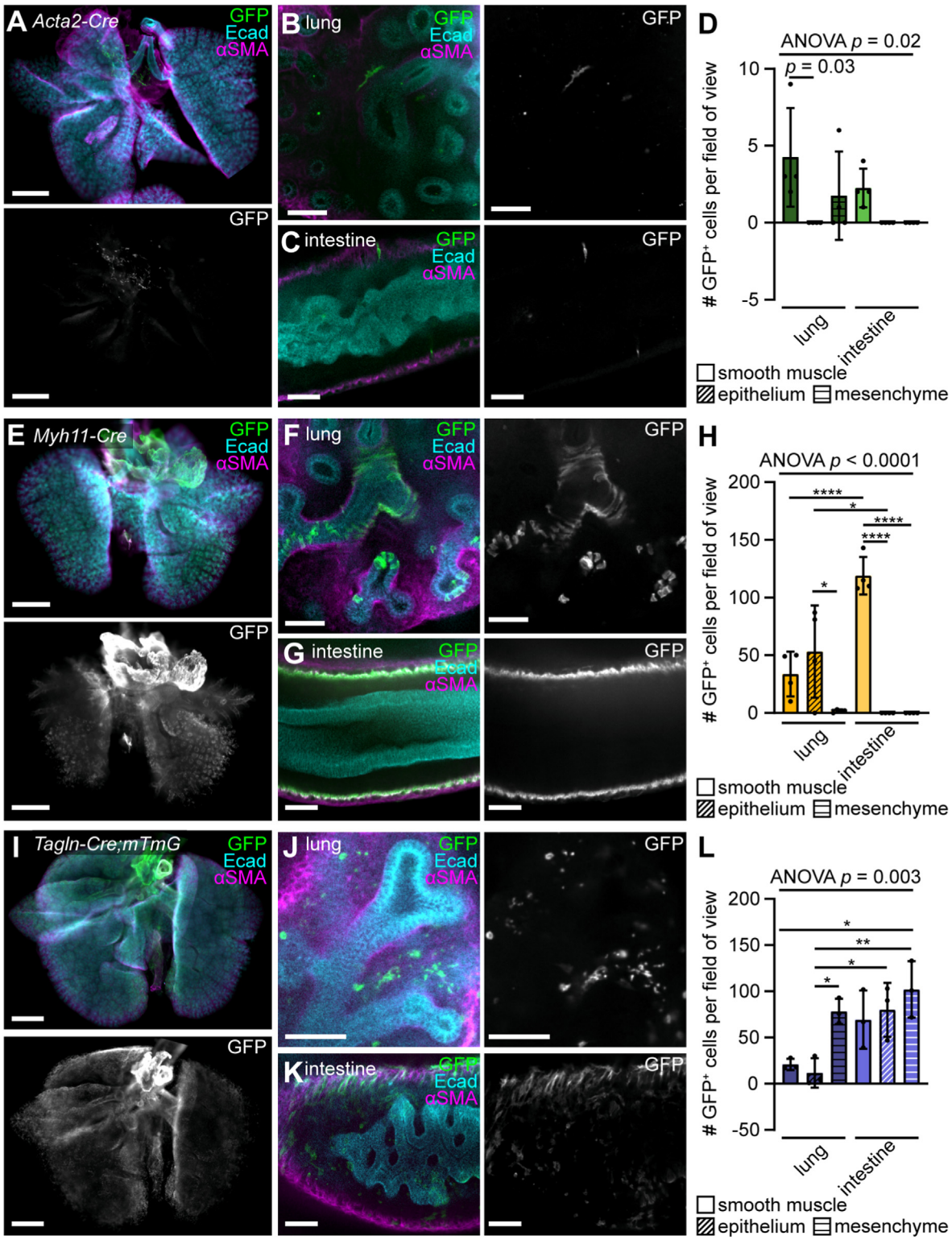

Fig. 5. Expression patterns of three smooth muscle-specific Cre lines in the embryonic lung and intestine at *E*15.5. (**A**) *E*15.5 *Acta2-Cre;mTmG* lungs immunostained for GFP, Ecad, and αSMA. Scale bars indicate 500 μm. (**B-C**) *E*15.5 *Acta2-Cre;mTmG* lung and intestine immunostained for GFP, Ecad, and αSMA. Scale bars indicate 50 μm. (**D**) Number of GFP^+ cells per field of view in the smooth muscle, epithelium, and mesenchyme of the lungs and intestine. (**E**) *E*15.5 *Myh11-Cre;mTmG* lungs immunostained for GFP, Ecad, and αSMA. Scale bars indicate 500 μm. (**F-G**) *E*15.5 *Myh11-Cre;mTmG* lungs and intestine immunostained for GFP, Ecad, and αSMA. Scale bars indicate 50 μm. (**H**) Number of GFP^+ cells per field of view in the smooth muscle, epithelium, and mesenchyme of the lungs and intestine. (**I**) *E*15.5 *Tagln-Cre;mTmG* lungs immunostained for GFP, Ecad, and αSMA. Scale bars indicate 500 μm. (**J-K**) *E*15.5 *Tagln-Cre;mTmG* lungs and intestine immunostained for GFP, Ecad, and αSMA. Scale bars indicate 50 μm. (**L**) Number of GFP^+ cells per field of view in the smooth muscle, epithelium, and mesenchyme of the lungs and intestine. *p* values obtained using ANOVA. Error bars show s.d.

within the epithelium (Fig. 4I-L). To confirm that *Acta2*, *Myh11*, and *Tagln* are not expressed in cell types other than smooth muscle in the embryonic lung and intestine, we examined published single-cell RNA-sequencing (scRNA-seq) datasets (Fazilaty et al., 2021; Goodwin et al., 2022a). We found that *Acta2*, *Myh11*, and *Tagln* are only expressed by smooth muscle cells of the lung at *E*11.5 and by smooth muscle cells of the intestine *E*14.5 (Fig. 4M–R). The patterns of GFP expression therefore indicate leakiness of these Cre lines, particularly in cell types of the embryonic lung.

We also examined later stages of development to determine whether the patterns of Cre expression are refined over developmental time. In *E*15.5 *Acta2-Cre;mTmG* lungs and intestines, we again found very few GFP^+ cells, indicating low Cre activity in these organs, despite the robust expression of αSMA (*Acta2*) (Fig. 5A–D). In *E*15.5 *Myh11-Cre;mTmG* lungs, we observed a surprising pattern of GFP^+ cells. While some smooth muscle cells were labelled, as intended, a large subset of epithelial cells were also GFP^+ (Fig. 5E–F, H). We observed this pattern in different lobes of the same lung and in lungs from different embryos, suggesting a high degree of leakiness of the *Myh11-Cre* driver. In contrast, we found that *E*15.5 *Myh11-Cre;mTmG* intestines have robust GFP expression in the smooth muscle layer and, unlike the lung, do not have any GFP^+ epithelial cells (Fig. 5G–H). Finally, we examined GFP expression in *E*15.5 *Tagln-Cre;mTmG* lungs and intestines. Similar to *E*12.5, we found sporadic GFP^+ cells in the mesenchyme, smooth muscle, and epithelium (Fig. 5I-L). Overall, these data show that none of the smooth muscle-specific Cre lines we investigated are active specifically or robustly in embryonic smooth muscle cells: *Acta2-Cre* activity is low, *Myh11-Cre* is higher but absent from early smooth muscle and often active in the airway epithelium, and *Tagln-Cre* is active in an apparently random set of cell types.

3.4. Smooth muscle-specific Cre lines show different levels of activity in vascular smooth muscle of the embryonic lung

The three Cre lines we explored here are also expected to target vascular smooth muscle. We therefore determined whether Cre was active in pulmonary vascular smooth muscle using the mTmG reporter. At *E*12.5, vascular smooth muscle is restricted to the proximal part of the lung and wraps the blood vessels running alongside the primary bronchi. *Acta2-Cre;mTmG* lungs lacked any GFP^+ cells in the vascular smooth muscle layer (Supplementary Fig. 1A), and *Myh11-Cre;mTmG* lungs showed sparse expression of GFP in vascular smooth muscle cells (Supplementary Fig. 1B). Consistent with the low levels of Cre activity in vascular smooth muscle at *E*12.5, *Acta2-Cre;DTA*$^{fl/+}$ and *Myh11-Cre;DTA*$^{fl/+}$ lungs have normal levels of vascular smooth muscle (arrowheads in Fig. 1A, G). Furthermore, *Acta2-Cre;DTA*$^{fl/+}$ and *Myh11-Cre;DTA*$^{fl/+}$ lungs appear completely normal at *E*15.5, suggesting that vascular smooth muscle was either not ablated or is not required for the pseudoglandular stages of lung development. *Tagln-Cre;mTmG* lungs showed the most GFP^+ cells within the vascular smooth muscle layer (Supplementary Fig. 1C), but the phenotype at *E*15.5 could not be confirmed because of embryonic lethality before *E*10.5. These three Cre lines therefore also appear to be unsuitable for studying the role of vascular smooth muscle in embryonic lung development.

4. Conclusions

Efforts to genetically ablate airway smooth muscle in the embryonic lung using DT-based mouse models were hampered by poor activity of smooth muscle-specific Cre drivers in the embryonic lung. The *Acta2-Cre* line was originally generated using the *Acta2* promoter and showed minimal activity in the adult kidney under healthy conditions and some activity in fibrosis (LeBleu et al., 2013). The *Myh11-Cre* line was generated using the *Myh11* promoter and included an EGFP reporter to visualize cells with Cre expression (Xin et al., 2002). EGFP is robustly expressed in the smooth muscle cells of many organs, but expression in epithelial cells has not previously been reported. The stark differences in *Myh11-Cre* activity in the embryonic lung and intestine are surprising and suggest that this line may be suitable for studies of intestinal but not airway smooth muscle. Finally, the *Tagln-Cre* line was generated using the *Tagln* promoter (Holtwick et al., 2002). The highest levels of Cre activity were detected in the aorta, intestine, and uterus, and Cre activity in non-smooth muscle cells has not been previously reported. The leakiness of this Cre line in both the embryonic lung and intestine suggest that it may not be suitable for studies of smooth muscle in these organs. There is an alternative *Tagln-Cre* line that was also generated using the *Tagln* promoter; a LacZ reporter shows that Cre is active in bronchial smooth muscle in the adult, but activity in the embryonic lung has not been examined (Lepore et al., 2005). To our knowledge, this line is not commercially available. The genomic locations of these transgenic insertions are unknown, raising the possibility that they are located in regions with minimal chromatin accessibility in the embryo, leading to very low expression of Cre recombinase despite high levels of expression of *Acta2, Myh11*, and *Tagln*. Similar issues with a lack of specificity and leakiness have been reported with the *Myh11-CreER*^{T2} line, which also causes transcriptomic changes in the murine aorta (Warthi et al., 2022).

To better target airway smooth muscle, Cre lines could be designed keeping in mind the temporal sequence in which genes are expressed during the smooth muscle differentiation trajectory (Goodwin et al., 2022a). Alternatively, introducing the sequence encoding Cre recombinase into the endogenous loci of genes of interest might lead to better matched patterns of Cre expression. Furthermore, the Cre lines we tested here are also expected to target vascular smooth muscle, making it difficult to isolate specific effects of airway smooth muscle. Overall, genetic strategies for targeting airway smooth muscle in the embryonic lung are sorely lacking, which complicates efforts to dissect the molecular and physical mechanisms by which this tissue influences the airway epithelium *in vivo*.

Author contributions

K.G. and C.M.N. conceptualized the study, designed the experiments, interpreted the data, and wrote the manuscript. K.G. performed the experiments and collected the data. Both authors provided input on the final manuscript.

Declaration of competing interest

The authors declare no competing interests.

Data availability

Data will be made available on request.

Acknowledgements

This work was supported in part by the NIH (HD099030, HL164861, HD111539) and a Faculty Scholars Award from the Howard Hughes Medical Institute. K.G. was supported in part by a postgraduate scholarship-doctoral (PGS-D) from the Natural Sciences and Engineering Research Council of Canada, the Dr. Margaret McWilliams Predoctoral Fellowship from the Canadian Federation of University Women, the Princeton University Procter Fellowship, and an American Heart Association Predoctoral Fellowship.

Appendix A. Supplementary data

Supplementary data to this article can be found online at https://doi.org/10.1016/j.ydbio.2023.01.008.

References

Buch, T., Heppner, F.L., Tertilt, C., Heinen, T.J., Kremer, M., Wunderlich, F.T., Jung, S., Waisman, A., 2005. A Cre-inducible diphtheria toxin receptor mediates cell lineage ablation after toxin administration. Nat. Methods 2, 419–426.

Butler, A., Hoffman, P., Smibert, P., Papalexi, E., Satija, R., 2018. Integrating single-cell transcriptomic data across different conditions, technologies, and species. Nat. Biotechnol. 36, 411–420.

Chen, J., Kitchen, C.M., Streb, J.W., Miano, J.M., 2002. Myocardin: a component of a molecular switch for smooth muscle differentiation. J. Mol. Cell. Cardiol. 34, 1345–1356.

Danopoulos, S., Alonso, I., Thornton, M.E., Grubbs, B.H., Bellusci, S., Warburton, D., Al Alam, D., 2018. Human lung branching morphogenesis is orchestrated by the spatiotemporal distribution of ACTA2, SOX2, and SOX9. Am. J. Physiol. Lung Cell Mol. Physiol. 314, L144–L149.

Donadon, M., Santoro, M.M., 2021. The Origin and Mechanisms of Smooth Muscle Cell Development in Vertebrates, 148. Development.

Du, K.L., Ip, H.S., Li, J., Chen, M., Dandre, F., Yu, W., Lu, M.M., Owens, G.K., Parmacek, M.S., 2003. Myocardin is a critical serum response factor cofactor in the transcriptional program regulating smooth muscle cell differentiation. Mol. Cell Biol. 23, 2425–2437.

Fazilaty, H., Brugger, M.D., Valenta, T., Szczerba, B.M., Berkova, L., Doumpas, N., Hausmann, G., Scharl, M., Basler, K., 2021. Tracing colonic embryonic transcriptional profiles and their reactivation upon intestinal damage. Cell Rep. 36, 109484.

Feng, H.Z., Wang, H., Takahashi, K., Jin, J.P., 2019. Double deletion of calponin 1 and calponin 2 in mice decreases systemic blood pressure with blunted length-tension response of aortic smooth muscle. J. Mol. Cell. Cardiol. 129, 49–57.

Goodwin, K., Jaslove, J.M., Tao, H., Zhu, M., Hopyan, S., Nelson, C.M., 2022a. Patterning the embryonic pulmonary mesenchyme. iScience 25, 103838.

Goodwin, K., Lemma, B., Zhang, P., Boukind, A., Nelson, C.M., 2022b. Plasticity in airway smooth muscle differentiation during mouse lung development. bioRxiv.

Goodwin, K., Mao, S., Guyomar, T., Miller, E., Radisky, D.C., Kosmrlj, A., Nelson, C.M., 2019. Smooth muscle differentiation shapes domain branches during mouse lung development. Development 146.

Goss, A.M., Tian, Y., Cheng, L., Yang, J., Zhou, D., Cohen, E.D., Morrisey, E.E., 2011. Wnt2 signaling is necessary and sufficient to activate the airway smooth muscle program in the lung by regulating myocardin/Mrtf-B and Fgf10 expression. Dev. Biol. 356, 541–552.

Hirashima, T., 2014. Pattern formation of an epithelial tubule by mechanical instability during epididymal development. Cell Rep. 9, 866–873.

Holtwick, R., Gotthardt, M., Skryabin, B., Steinmetz, M., Potthast, R., Zetsche, B., Hammer, R.E., Herz, J., Kuhn, M., 2002. Smooth muscle-selective deletion of guanylyl cyclase-A prevents the acute but not chronic effects of ANP on blood pressure. Proc. Natl. Acad. Sci. U. S. A. 99, 7142–7147.

Honjo, T., Nishizuka, Y., Kato, I., Hayaishi, O., 1971. Adenosine diphosphate ribosylation of aminoacyl transferase II and inhibition of protein synthesis by diphtheria toxin. J. Biol. Chem. 246, 4251–4260.

Hung, C.F., Chow, Y.H., Liles, W.C., Altemeier, W.A., Schnapp, L.M., 2017. Ablation of pericyte-like cells in lungs by oropharyngeal aspiration of diphtheria toxin. Am. J. Respir. Cell Mol. Biol. 56, 160–167.

Huycke, T.R., Miller, B.M., Gill, H.K., Nerurkar, N.L., Sprinzak, D., Mahadevan, L., Tabin, C.J., 2019. Genetic and mechanical regulation of intestinal smooth muscle development. Cell 179, 90–105 e121.

Ivanova, A., Signore, M., Caro, N., Greene, N.D., Copp, A.J., Martinez-Barbera, J.P., 2005. In vivo genetic ablation by Cre-mediated expression of diphtheria toxin fragment A. Genesis 43, 129–135.

Jaslove, J.M., Nelson, C.M., 2018. Smooth muscle: a stiff sculptor of epithelial shapes. Philos. Trans. R. Soc. Lond. B Biol. Sci. 373.

Kim, H.Y., Pang, M.F., Varner, V.D., Kojima, L., Miller, E., Radisky, D.C., Nelson, C.M., 2015. Localized smooth muscle differentiation is essential for epithelial bifurcation during branching morphogenesis of the mammalian lung. Dev. Cell 34, 719–726.

LeBleu, V.S., Taduri, G., O'Connell, J., Teng, Y., Cooke, V.G., Woda, C., Sugimoto, H., Kalluri, R., 2013. Origin and function of myofibroblasts in kidney fibrosis. Nat. Med. 19, 1047–1053.

Lepore, J.J., Cheng, L., Min Lu, M., Mericko, P.A., Morrisey, E.E., Parmacek, M.S., 2005. High-efficiency somatic mutagenesis in smooth muscle cells and cardiac myocytes in SM22alpha-Cre transgenic mice. Genesis 41, 179–184.

Schildmeyer, L.A., Braun, R., Taffet, G., Debiasi, M., Burns, A.E., Bradley, A., Schwartz, R.J., 2000. Impaired vascular contractility and blood pressure homeostasis in the smooth muscle alpha-actin null mouse. Faseb. J. 14, 2213–2220.

Schneider, C.A., Rasband, W.S., Eliceiri, K.W., 2012. NIH Image to ImageJ: 25 years of image analysis. Nat. Methods 9, 671–675.

Shyer, A.E., Tallinen, T., Nerurkar, N.L., Wei, Z., Gil, E.S., Kaplan, D.L., Tabin, C.J., Mahadevan, L., 2013. Villification: how the gut gets its villi. Science 342, 212–218.

Solway, J., Seltzer, J., Samaha, F.F., Kim, S., Alger, L.E., Niu, Q., Morrisey, E.E., Ip, H.S., Parmacek, M.S., 1995. Structure and expression of a smooth muscle cell-specific gene, SM22 alpha. J. Biol. Chem. 270, 13460–13469.

Stuart, T., Butler, A., Hoffman, P., Hafemeister, C., Papalexi, E., Mauck 3rd, W.M., Hao, Y., Stoeckius, M., Smibert, P., Satija, R., 2019. Comprehensive integration of single-cell data. Cell 177, 1888–1902 e1821.

Wang, Z., Wang, D.Z., Pipes, G.C., Olson, E.N., 2003. Myocardin is a master regulator of smooth muscle gene expression. Proc. Natl. Acad. Sci. U. S. A. 100, 7129–7134.

Warthi, G.D., Faulkner, J.L., Doja, J., Ghanam, A.R., Gao, P., Yang, A.C., Slivano, O.J., Barris, C.T., Kress, T.C., Zawieja, S.D., Griffin, S.H., Xie, X., Ashworth, A., Christie, C.K., Bryant, W.B., Kumar, A., Davis, M.J., Long, X., Gan, L., Belin de Chantemèle, E.J., Lyu, Q., Miano, J.M., 2022. Generation and comparative analysis of an Itga8-CreERT2 mouse with preferential activity in vascular smooth muscle cells. Nat. Cardiovasc. Res. 1, 1084–1100.

Xin, H.B., Deng, K.Y., Rishniw, M., Ji, G., Kotlikoff, M.I., 2002. Smooth muscle expression of Cre recombinase and eGFP in transgenic mice. Physiol. Genom. 10, 211–215.

Yang, Y., Paivinen, P., Xie, C., Krup, A.L., Makela, T.P., Mostov, K.E., Reiter, J.F., 2021. Ciliary Hedgehog signaling patterns the digestive system to generate mechanical forces driving elongation. Nat. Commun. 12, 7186.

Young, R.E., Jones, M.K., Hines, E.A., Li, R., Luo, Y., Shi, W., Verheyden, J.M., Sun, X., 2020. Smooth muscle differentiation is essential for airway size, tracheal cartilage segmentation, but dispensable for epithelial branching. Dev. Cell 53, 73–85 e75.

Zhang, J.C., Kim, S., Helmke, B.P., Yu, W.W., Du, K.L., Lu, M.M., Strobeck, M., Yu, Q., Parmacek, M.S., 2001. Analysis of SM22alpha-deficient mice reveals unanticipated insights into smooth muscle cell differentiation and function. Mol. Cell Biol. 21, 1336–1344.

Zuo, W., Zhang, T., Wu, D.Z., Guan, S.P., Liew, A.A., Yamamoto, Y., Wang, X., Lim, S.J., Vincent, M., Lessard, M., Crum, C.P., Xian, W., McKeon, F., 2015. p63(+) Krt5(+) distal airway stem cells are essential for lung regeneration. Nature 517, 616–620.